


Direct Calculation of the Interfacial Free Energy between NaCl Crystal and Its Aqueous Solution at the Solubility Limit

Ignacio Sanchez-Burgos¹ and Jorge R. Espinosa^{1*}

*Maxwell Centre, Cavendish Laboratory, Department of Physics, University of Cambridge,
J J Thomson Avenue, Cambridge CB3 0HE, United Kingdom*

 (Received 17 August 2022; revised 7 November 2022; accepted 30 January 2023; published 15 March 2023)

Salty water is the most abundant electrolyte aqueous mixture on Earth, however, very little is known about the NaCl-saturated solution interfacial free energy (γ_s). Here, we provide the first direct estimation of γ_s for several NaCl crystallographic planes by means of the mold integration technique, a highly efficient computational method to evaluate interfacial free energies with anisotropic crystal resolution. Making use of the JC-SPC/E model, one of the most benchmarked force fields for NaCl water solutions, we measure γ_s of four different crystal planes, (100), (110), (111), and (11 $\bar{2}$) with the saturated solution at normal conditions. We find high anisotropy between the different crystal orientations with values ranging from 100 to 150 mJ m⁻², and the average value of the distinct planes being $\bar{\gamma}_s = 137(20)$ mJ m⁻². This value for the coexistence interfacial free energy is in reasonable agreement with previous extrapolations from nucleation studies. Our Letter represents a milestone in the computational calculation of interfacial free energies between ionic crystals and aqueous solutions.

DOI: [10.1103/PhysRevLett.130.118001](https://doi.org/10.1103/PhysRevLett.130.118001)

Electrolyte solutions, and more specifically NaCl solutions, are ubiquitous, with sodium chloride being the major component of sea salt [1] and atmospheric aerosols [2], as well as playing a key role in atmospheric chemistry [3]. At salt concentrations greater than the solubility, crystals of the ionic salt can be formed, giving rise to a liquid-solid interface. The amount of energy per unit of area required to form such interface is known as the interfacial free energy (γ_s). However, despite the fact that this magnitude is highly relevant in controlling salt precipitation, no experimental techniques have been able to accurately measure γ_s for planar liquid-solid interfaces [4,5]. Therefore, computational techniques can be useful to provide guidance on such important magnitude.

Computational approaches to directly evaluate the liquid-crystal γ_s include cleaving [6], tethered Monte Carlo [7], metadynamics [8], mold integration [9], capillary wave fluctuations [10], and other related thermodynamic integration schemes [11–13]. These techniques have been proven to provide reliable estimates of the liquid-solid interfacial free energy for different crystallographic planes and numerous soft matter systems [14–23]. However, for the case of the NaCl-saturated water solution interface, none of these methods have yet been implemented due to their high computational cost. Currently, the only available estimates of γ_s for the NaCl aqueous solution have been obtained at deep supersaturation via computational nucleation studies using seeding [24] and forward flux sampling [25], as well as through experimental measurements of the nucleation rate [26]. Then, by means of the classical nucleation theory (CNT) [27,28], γ_s has been estimated for curved interfaces

under supersaturation conditions. By extrapolating such results to the saturation concentration, we find the first approximation to the crystal NaCl aqueous solution γ_s at coexistence conditions. However, this is not an entirely satisfactory approach given that it relies on the CNT framework, order parameters to identify the number of particles in the clusters [29], and does not provide any anisotropic crystal information on γ_s .

In this Letter, we directly evaluate the interfacial free energy at normal conditions between the NaCl crystal and its aqueous solution at the solubility limit for different crystal planes: (100), (110), (111), and (11 $\bar{2}$). We choose the simple point charge/extended (SPC/E) water model [30] in combination with the Joung-Cheetham parametrization (JC) for Na⁺ and Cl⁻ ions [31] (further details on the force field parameters and simulation setups can be found in Supplemental Material, SM [32]) since it can reasonably reproduce the experimental behavior of NaCl aqueous solutions [31,46,47]. Moreover, this model has been extensively used to benchmark solubility calculations employing different techniques [48–51], resulting in a solubility of $m = 3.71$ mol kg⁻¹ [52], moderately lower than the experimental one, 6.15 mol kg⁻¹. We use the GROMACS Molecular Dynamics package [36] in combination with the mold integration (MI) technique [9], where the formation of a solid slab in the solution is performed along a reversible pathway, and the free energy difference between the initial (aqueous solution) and final state (aqueous solution + crystal slab) corresponds to γ_s times the area of the induced liquid-solid interface. Through MI, γ_s can be obtained as

$$\gamma_s = \frac{1}{2A} \left(\varepsilon_m N_w - \int_0^{\varepsilon_m} d\varepsilon \langle N(\varepsilon) \rangle \right), \quad (1)$$

where ε is the energy of the potential wells (and ε_m the maximum depth employed), A is the surface of the liquid-solid interface, N_w the number of wells in the mold, and $\langle N(\varepsilon) \rangle$ the average number of occupied wells at a given potential energy depth value. The method consists on performing thermodynamic integration (TI) along the path in which the depth of the mold potential wells is gradually increased to a maximum value of ε_m . To ensure reversibility in Eq. (1), the crystal structure induced by the mold must quickly melt when the interaction between the potential wells and the fluid is switched off. Consequently, the TI has to be performed at well radii (r_w) that are wider than the optimal one, r_w^o , at which the crystal slab is fully formed, and therefore can possibly induce irreversible crystal growth (i.e., leading to an overestimation of $\langle N(\varepsilon) \rangle$). Therefore, $\gamma_s(r_w)$ is estimated for several values of $r_w > r_w^o$, and then, extrapolated to r_w^o , which is the well radius that recovers the exact free energy value γ_s [9,14–17]. In practice, the method consists of two distinct steps [9]: in the first one, we find r_w^o by performing several simulations in which we identify the largest well width at which the induced solid layer grows or keeps stable without melting (i.e., $r_w < r_w^o$). In the second step, multiple simulations at radii wider than the optimal one are performed, and we measure the average number of wells occupied for each radius as a function of ε to solve Eq. (1).

In Fig. 1, we describe such procedure for the (11 $\bar{2}$) crystal plane at $T = 298$ K and $p = 1$ bar. First, to determine r_w^o , we develop a configuration in which the NaCl crystal positions of the mold are already occupied

with their corresponding type of ions [Fig. 1(a)]. Additionally, a crystal layer displaying vacancies (randomly located) in half of the Na⁺/Cl⁻ lattice positions is placed at each side of the inserted mold. Importantly, the ions within such adjacent two semioccupied crystal layers are not held through potential wells to retain their equilibrium lattice positions. Since the crystal growth of the NaCl solid at solubility conditions is extremely slow [49], especially for crystal planes with low Miller indices [such as the (100) [53]], we can estimate r_w^o in the limit at which each of the adjacent half layers of NaCl ions to the potential mold dissolves or not. If they melt, the potential wells are too wide to induce crystallization, whereas if the ions of the layers aside the mold remain crystalline over long timescales (or even grow), such value of r_w is considered below the optimal radius. Importantly, to ensure that the solution concentration remains constant at $m \sim 3.7$ mol kg⁻¹ despite partial melting or growth from the crystal slab [Fig. 1(b)], we employ system sizes with over 10 000 water molecules, which can absorb small variations of ions from the slab to the solution or vice versa [Fig. 1(a)]. We use the isothermal-isobaric (NpT) ensemble—where pressure is only applied to the perpendicular axis to the crystal-liquid interface—to keep constant both temperature and pressure. We note that an alternative approach to keep constant the solution concentration in our MD simulations without requiring an elongated box is through the grand canonical ensemble [54,55]. Nevertheless, it may have only sped up our simulations by a factor of 3 since system sizes of at least 3500 molecules would have been still needed to prevent finite size effects in our MI calculations [9,14].

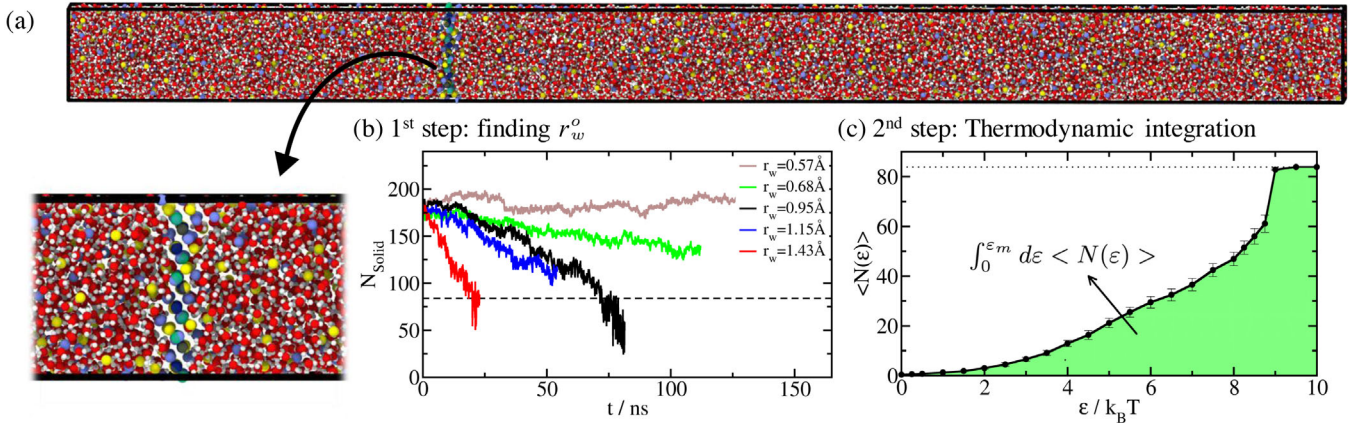


FIG. 1. Determination of γ_s for the (11 $\bar{2}$) crystal plane: (a) Representative simulation box employed for the MI technique along with a close view of the mold occupied by ions. The images were rendered using ovitto [56]. (b) First step of the MI calculation to determine the optimal well radius (r_w^o): time evolution of the number of ions conforming the NaCl crystal slab is depicted for different well widths (r_w). The horizontal dashed line indicates the total number of ions that can be accommodated within the mold. N_{solid} was determined through the \bar{q}_4 - \bar{q}_6 local order parameter [57] (further details in SM [32]). (c) Second step of MI calculations: simulations at different well depth (ε) values for a fixed r_w are performed to evaluate the integral from Eq. (1). The average number of occupied wells $\langle N(\varepsilon) \rangle$ against ε is plotted here for $r_w = 0.78$ Å. The green shaded area gives the integral of Eq. (1).

In Fig. 1(b), we show the time evolution of solid-like ions (evaluated through the $\bar{q}_4\text{-}\bar{q}_6$ local order parameter [57]; further details on SM [32]) for different well widths of the $(11\bar{2})$ plane. Here, well radii greater than 0.68 \AA results in gradual dissolution of the crystal layers located at each side of the crystal plane induced by the mold. However, for $r_w = 0.57 \text{ \AA}$ those ions remain ordered aside the crystal slab and even mildly grow over time, hence indicating that such r_w is lower than r_w^o . Therefore, we determine r_w^o at the intermediate value of 0.625 \AA .

Once r_w^o has been determined, we perform TI to compute the required free energy to induce the formation of the crystal slab. TI requires performing simulations at different well depths (ϵ) for a fixed r_w and measuring the average occupation of the mold at each ϵ , which is the integrand of Eq. (1). To minimize the extent of irreversibility (due to crystal growth) in these calculations, we integrate at r_w values of 0.78 and 0.92 \AA . In Fig. 1(c) we show the average number of occupied wells as a function of the well depth (ϵ) for $r_w = 0.78 \text{ \AA}$, where the shaded area corresponds to the integral in Eq. (1), from which we can directly obtain the interfacial free energy. In Sec. SII of SM [32] we include a detailed discussion of the different sources of uncertainty along the integration pathway, including the small hysteresis associated with the steep change in $\langle N(\epsilon) \rangle$ at the mold high occupation regime (Fig. S2). Once γ_s is evaluated for different r_w values, it can be extrapolated to the optimal r_w^o . In Fig. 2 we show the obtained interfacial free energy for $r_w > r_w^o$ depicted with filled symbols, along with the corresponding extrapolations to the optimal radius, represented by empty symbols. Apart from the $(11\bar{2})$ plane, we also evaluate γ_s for the (100), (110), and (111) planes. For all planes we follow the same procedure described for the $(11\bar{2})$ face. The final interfacial free energies for the different planes are reported in Table I, where we also

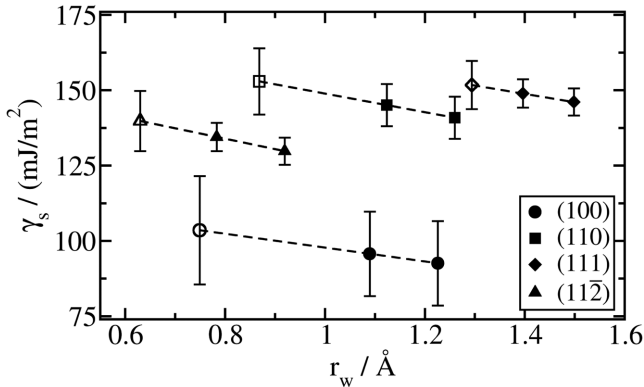


FIG. 2. Interfacial free energy as a function of the potential well radius evaluated for four different crystal orientations. Filled symbols indicate γ_s obtained through Eq. (1) for $r_w > r_w^o$, while dashed lines depict linear extrapolations to the optimal well radius r_w^o (empty symbols).

include the planar density as the number of ions per nanometer², as well as the total number of potential wells employed for the calculation of each crystal plane. For all the different orientations, we make use of two layers of potential wells to induce the formation of the crystal slab. For reproducibility purposes, in SM [32] we provide source data links to all the liquid-crystal and pure NaCl solid configurations employed in our MI calculations, along with snapshots of the four planes studied (Fig. S3).

Strikingly, when comparing the interfacial free energy of the distinct crystal orientations (Fig. 2), we find large differences, of up to 50% higher values, for the (110) and (111) planes compared to the (100) face (Table I); showing high resemblance to the anisotropy found in the crystal-molten NaCl interfacial free energy (although with the Tosi-Fumi model [15]). However, while the differences in γ_s between these distinct planes in crystal-molten NaCl were of the order of $5\text{--}15 \text{ mJ m}^{-2}$ [15,18], in NaCl aqueous solutions they can reach up to $40\text{--}50 \text{ mJ m}^{-2}$. We note that within the uncertainty of our calculations (Table I), the anisotropy in γ_s is only statistically significant between the (100) plane and the (110) and (111) crystal orientations. The higher interfacial anisotropy in NaCl aqueous solutions is also consistent with the fact that the average γ_s for the studied planes ($\bar{\gamma}_s$) is $\sim 137 \text{ mJ m}^{-2}$, whereas for the crystal-molten NaCl is between $90\text{--}100 \text{ mJ m}^{-2}$ [15,18]. This is a reasonable result given that in the crystal-molten interface, both phases are formed by particles of the same nature (Na^+ and Cl^- ions) and, therefore, the energetic cost to form an interface should be lower [58]. Nonetheless, the crystal-molten NaCl calculations were performed for the Tosi-Fumi model at its coexistence temperature (1082 K), and therefore, this cannot be taken as a direct comparison.

By applying a Wulff's construction [59,60] (further details provided in SM [32]), we also determine the shape of the macroscopic NaCl crystals through our calculations, and estimate an average value of the interfacial free energy for such crystals ($\gamma_{s,W} = 109 \text{ mJ m}^{-2}$). The lower average value of $\gamma_{s,W}$ obtained via the Wulff's construction compared to $\bar{\gamma}_s$ can be explained through the much greater contribution of the (100) plane to the macroscopic crystal

TABLE I. Values of the ion density per layer, number of potential wells (N_w) employed in the MI calculations, and the resulting liquid-solid interfacial free energy (γ_s) for each of the studied crystal orientations. $\bar{\gamma}_s$ represents the average of the different crystal orientations.

Crystal plane	Layer density/(ions nm^{-2})	N_w	$\gamma_s/(\text{mJ m}^{-2})$
(100)	11.967	200	104 ± 18
(110)	8.462	140	153 ± 11
(111)	6.909	112	152 ± 8
($11\bar{2}$)	4.885	84	140 ± 10
Average $\bar{\gamma}_s =$			$137 \pm 20 \text{ mJ m}^{-2}$

compared to the rest of crystal orientations studied here. Moreover, in reasonable agreement with experiments [61], the predicted shape by the JC-SPC/E model for the macroscopic NaCl crystal is roughly cubic with the corners cut out by the exposure of the $(11\bar{2})$ plane (Fig. S4).

Interestingly, we also note that there is no clear correlation between the plane density and interfacial free energy of the studied orientations (Table I), in contrast to some previously investigated systems such as Hard-Spheres [20,62–64] or Lennard-Jones [9,19,65]. The reason behind such observation in Hard-Spheres or Lennard-Jones systems is that higher planar density usually implies higher differences in density between the lower density coexisting liquid and the higher density crystal phase. However, in NaCl aqueous solutions, although such behavior also applies, the delicate balance between electrostatic repulsion and ion ordering might additionally modulate γ_s .

We compare our values of γ_s at the solubility concentration with those previously estimated from nucleation studies at high supersaturation. From both experimental [26] and computational [24,25,29] nucleation rates, an average of γ_s (for a curved interface containing contributions of all the possible crystal orientations) can be inferred by means of the Classical Nucleation Theory [27,28]. Importantly, since most of the previous computational nucleation studies were performed using the JC-SPC/E model [24,25,29], we can establish a direct comparison of our results to those from supersaturated concentrations. In Fig. 3, we plot the interfacial free energy as a function of supersaturation (S). Our results for γ_s at coexistence are shown for each of the crystal orientation that we studied (empty triangles) together

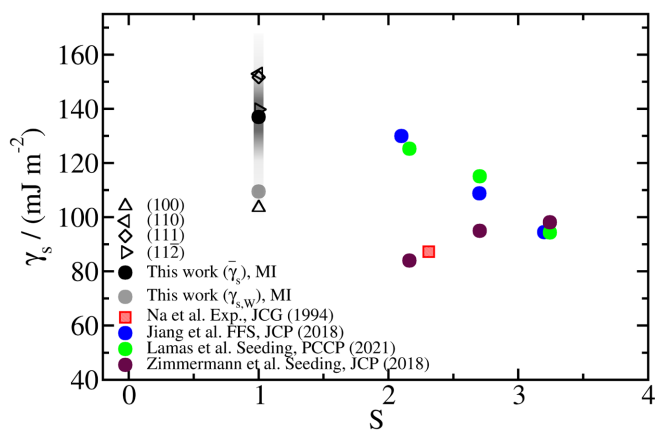


FIG. 3. Interfacial free energy (γ_s) as a function of supersaturation ($S = m/m_{\text{sat}}$), being $m_{\text{sat}} = 3.71 \text{ mol kg}^{-1}$ for the JC-SPC/E model, and 6.15 mol kg^{-1} for the experimental data. Our calculations at $S = 1$ for different crystal orientations (empty triangles) as well as for $\bar{\gamma}_s$ and $\gamma_{s,W}$ (filled circles) are depicted by black and gray symbols, respectively. Interfacial free energies obtained from nucleation studies at high supersaturations, both computational [24,25,29] and experimental [26], are also included as indicated in the legend.

with the mean value of them ($\bar{\gamma}_s$; black circle) and the average value from the Wulff’s construction for the equilibrium crystal ($\gamma_{s,W}$; gray circle). As can be seen, the extrapolated interfacial free energy trend to $S = 1$ from Lamas *et al.* [24] and Jiang *et al.* [25] are in excellent agreement with our direct calculations of γ_s for different crystal planes. However, a significant better agreement is found between the extrapolated interfacial free energy from these nucleation studies and $\bar{\gamma}_s$ (arithmetic mean) than with the obtained $\gamma_{s,W}$ from the Wulff’s construction (Fig. 3). That might be explained by the fact that in nucleation studies the typical size of the NaCl clusters is of the order of tens of ions (i.e., from 10 to 100 ions [24,25,29]), and their shape is roughly spherical. Hence, the overall γ_s for these small critical nuclei may be contributed by different crystallographic planes, interfacial defects, curvature effects, or by the Laplace pressure [49,66]. In fact, even large critical nuclei stable at much less supersaturated concentrations (i.e., $S \sim 1.5$) typically display spherical shapes which may exhibit curvature effects [49]. In contrast, at the saturation concentration, macroscopic roughly cubic crystals mainly exposing the (100) plane [with a possible small contribution of the $(11\bar{2})$, or (111) planes on the vertices [61]] are expected to be formed displaying an overall interfacial free energy that highly resembles that of the (100) plane: $\gamma_{s,W} = 109 \text{ mJ m}^{-2}$ vs $\gamma_{s,(100)} = 104 \text{ mJ m}^{-2}$. Such a mostly cubic shape of the equilibrium NaCl crystal predicted through the Wulff’s construction (Fig. S4) is in good agreement with experimental observations for macroscopic NaCl crystallites [61,67].

On the contrary, the extrapolated trend from Zimmermann *et al.* [29] significantly underestimates $\bar{\gamma}_s$ and $\gamma_{s,W}$ at coexistence conditions (Fig. 3). That is not surprising considering that the nucleation rates from which the interfacial free energies were obtained in Ref. [29] severely overestimated those from Refs. [24,25]. Importantly, the γ_s dependence with supersaturation which reasonably extrapolates to our calculations (those from Refs. [24,25]) suggests that γ_s decreases as the salt concentration increases. This observation would be consistent with the fact that the chemical composition of both phases becomes increasingly similar with supersaturation, and thus, at the limit of infinite supersaturation (molten NaCl), the interfacial free energy should be lower than at the solubility limit [15]. The observed substantial differences in γ_s from nucleation studies also evidence the critical relevance of the employed local order parameter for determining the nucleus size, and thus, the interfacial free energy [29]. Finally, we also compare with the experimental interfacial free energy inferred by Na *et al.* [26] using the CNT framework (Fig. 3, red square), which is significantly below the predicted γ_s from Refs. [24,25] (not from Ref. [29]), although it is qualitatively consistent with the hypothesis that the interfacial free energy may decrease with supersaturation. A simple possible explanation for the observed discrepancies

between these computational vs experimental nucleation estimates of γ_s may be the force field performance, nevertheless, the difficult determination of the experimental CNT kinetic prefactor to infer the nucleation free energy barrier, from which the interfacial free energy is ultimately extracted, might also add a significant degree of uncertainty.

In summary, we provide here the first direct measurement of the NaCl–brine solution interfacial free energy at the saturation concentration and normal conditions. We overcome inherent difficulties of these calculations, such as the slow crystal growth dynamics, by employing mold integration, a computational technique which evaluates the free energy work to form a crystal slab from the saturated solution. By using the JC-SPC/E model, one of the most benchmarked force fields for NaCl in water, we measure the interfacial free energy of four different planes: the (100), (110), (111), and (11 $\bar{2}$); obtaining an average value of $\bar{\gamma}_s = 137(20)$ mJ m $^{-2}$. Remarkably, large differences of up to 50 mJ m $^{-2}$ in γ_s between the different crystal orientations are found. Finally, we note that our results of γ_s at the solubility limit are consistent with extrapolated values from nucleation studies (using the same model) as well as with experimental data inferred from a CNT analysis at high supersaturation. Taken together, this Letter represents a milestone in the computational calculation of interfacial free energies between aqueous solutions and ionic crystals.

This project has received funding from the Oppenheimer Research Fellowship of the University of Cambridge. I. S.-B. acknowledges funding from the Derek Brewer scholarship of Emmanuel College and EPSRC Doctoral Training Programme studentship, No. EP/T517847/1. J. R. E. also acknowledges funding from the Roger Ekins Research Fellowship of Emmanuel College, and the Ramon y Cajal Fellowship (RYC2021-030937-I). This work has been performed using 3 million CPU hours provided by the Cambridge Tier-2 system operated by the University of Cambridge Research Computing Service funded by the EPSRC Tier-2 capital grant EP/P020259/1. We thank V. Roser for critical reading of the manuscript.

*To whom correspondence should be addressed.
jr752@cam.ac.uk

- [1] J. Lyman and R. H. Fleming, Composition of sea water, *J. Mar. Res.* **3**, 134 (1940).
- [2] U. Pöschl, Atmospheric aerosols: Composition, transformation, climate and health effects, *Angew. Chem., Int. Ed.* **44**, 7520 (2005).
- [3] S. T. Martin, Phase transitions of aqueous atmospheric particles, *Chem. Rev.* **100**, 3403 (2000).
- [4] L. Ickes, A. Welti, C. Hoose, and U. Lohmann, Classical nucleation theory of homogeneous freezing of water: Thermodynamic and kinetic parameters, *Phys. Chem. Chem. Phys.* **17**, 5514 (2015).
- [5] R. Bahadur, L. M. Russell, and S. Alavi, Surface tensions in NaCl- water- air systems from MD simulations, *J. Phys. Chem. B* **111**, 11989 (2007).
- [6] J. Q. Broughton and G. H. Gilmer, Molecular dynamics investigation of the crystal–fluid interface. VI. Excess surface free energies of crystal–liquid systems, *J. Chem. Phys.* **84**, 5759 (1986).
- [7] L. A. Fernández, V. Martin-Mayor, B. Seoane, and P. Verrocchio, Equilibrium Fluid-Solid Coexistence of Hard Spheres, *Phys. Rev. Lett.* **108**, 165701 (2012).
- [8] S. Angioletti-Uberti, M. Ceriotti, P. D. Lee, and M. W. Finnis, Solid-liquid interface free energy through metadynamics simulations, *Phys. Rev. B* **81**, 125416 (2010).
- [9] J. Espinosa, C. Vega, and E. Sanz, The mold integration method for the calculation of the crystal-fluid interfacial free energy from simulations, *J. Chem. Phys.* **141**, 134709 (2014).
- [10] J. J. Hoyt, M. Asta, and A. Karma, Method for Computing the Anisotropy of the Solid-Liquid Interfacial Free Energy, *Phys. Rev. Lett.* **86**, 5530 (2001).
- [11] R. Benjamin and J. Horbach, Crystal-liquid interfacial free energy via thermodynamic integration, *J. Chem. Phys.* **141**, 044715 (2014).
- [12] T. Schilling and F. Schmid, Computing absolute free energies of disordered structures by molecular simulation, *J. Chem. Phys.* **131**, 231102 (2009).
- [13] M. Bültmann and T. Schilling, Computation of the solid-liquid interfacial free energy in hard spheres by means of thermodynamic integration, *Phys. Rev. E* **102**, 042123 (2020).
- [14] I. Sanchez-Burgos, E. Sanz, C. Vega, and J. R. Espinosa, FCC vs. HCP competition in colloidal hard-sphere nucleation: On their relative stability, interfacial free energy and nucleation rate, *Phys. Chem. Chem. Phys.* **23**, 19611 (2021).
- [15] J. R. Espinosa, C. Vega, C. Valeriani, and E. Sanz, The crystal-fluid interfacial free energy and nucleation rate of NaCl from different simulation methods, *J. Chem. Phys.* **142**, 194709 (2015).
- [16] J. R. Espinosa, C. Vega, and E. Sanz, Ice–water interfacial free energy for the TIP4P, TIP4P/2005, TIP4P/Ice, and mW models as obtained from the mold integration technique, *J. Phys. Chem. C* **120**, 8068 (2016).
- [17] G. D. Soria, J. R. Espinosa, J. Ramirez, C. Valeriani, C. Vega, and E. Sanz, A simulation study of homogeneous ice nucleation in supercooled salty water, *J. Chem. Phys.* **148**, 222811 (2018).
- [18] J. Benet, L. G. MacDowell, and E. Sanz, Interfacial free energy of the NaCl crystal-melt interface from capillary wave fluctuations, *J. Chem. Phys.* **142**, 134706 (2015).
- [19] R. L. Davidchack and B. B. Laird, Direct calculation of the crystal–melt interfacial free energies for continuous potentials: Application to the Lennard-Jones system, *J. Chem. Phys.* **118**, 7651 (2003).
- [20] R. L. Davidchack, Hard spheres revisited: Accurate calculation of the solid–liquid interfacial free energy, *J. Chem. Phys.* **133**, 234701 (2010).
- [21] M. Ambler, B. Vorselaars, M. P. Allen, and D. Quigley, Solid-liquid interfacial free energy of ice ih, ice ic, and ice 0 within a mono-atomic model of water via the capillary wave method, *J. Chem. Phys.* **146**, 074701 (2017).

- [22] M. Asta, J. Hoyt, and A. Karma, Calculation of alloy solid-liquid interfacial free energies from atomic-scale simulations, *Phys. Rev. B* **66**, 100101(R) (2002).
- [23] J. Algaba, E. Acuña, J. M. Míguez, B. Mendiboure, I. M. Zerón, and F. J. Blas, Simulation of the carbon dioxide hydrate-water interfacial energy, *J. Colloid Interface Sci.* **623**, 354 (2022).
- [24] C. Lamas, J. Espinosa, M. Conde, J. Ramírez, P. M. de Hijes, E. G. Noya, C. Vega, and E. Sanz, Homogeneous nucleation of NaCl in supersaturated solutions, *Phys. Chem. Chem. Phys.* **23**, 26843 (2021).
- [25] H. Jiang, A. Haji-Akbari, P. G. Debenedetti, and A. Z. Panagiotopoulos, Forward flux sampling calculation of homogeneous nucleation rates from aqueous NaCl solutions, *J. Chem. Phys.* **148**, 044505 (2018).
- [26] H.-S. Na, S. Arnold, and A. S. Myerson, Cluster formation in highly supersaturated solution droplets, *J. Cryst. Growth* **139**, 104 (1994).
- [27] M. Volmer and A. Weber, Keimbildung in übersättigten gebilden, *Z. Phys. Chem.* **119**, 277 (1926).
- [28] R. Becker and W. Döring, Kinetische behandlung der keimbildung in übersättigten dampfen, *Ann. Phys. (Berlin)* **416**, 719 (1935).
- [29] N. E. Zimmermann, B. Vorselaars, J. R. Espinosa, D. Quigley, W. R. Smith, E. Sanz, C. Vega, and B. Peters, NaCl nucleation from brine in seeded simulations: Sources of uncertainty in rate estimates, *J. Chem. Phys.* **148**, 222838 (2018).
- [30] H. Berendsen, J. Grigera, and T. Straatsma, The missing term in effective pair potentials, *J. Phys. Chem.* **91**, 6269 (1987).
- [31] I. S. Joung and T. E. Cheatham III, Molecular dynamics simulations of the dynamic and energetic properties of alkali and halide ions using water-model-specific ion parameters, *J. Phys. Chem. B* **113**, 13279 (2009).
- [32] See Supplemental Material at <http://link.aps.org/supplemental/10.1103/PhysRevLett.130.118001> for further details on the force field parameters and simulation methods, which includes Refs. [33–45].
- [33] H. A. Lorentz, Ueber die anwendung des satzes vom virial in der kinetischen theorie der gase, *Ann. Phys. (Berlin)* **248**, 127 (1881).
- [34] D. Berthelot, Sur une méthode purement physique pour la détermination des poids moléculaires des gaz et des poids atomiques de leurs éléments, *J. Phys. Théor. Appl.* **8**, 263 (1899).
- [35] I. M. Zeron, J. M. Míguez, B. Mendiboure, J. Algaba, and F. J. Blas, Simulation of the CO₂ hydrate-water interfacial energy: The mold integration-guest methodology, *J. Chem. Phys.* **157**, 134709 (2022).
- [36] H. Bekker, H. Berendsen, E. Dijkstra, S. Achterop, R. Vondrumen, D. VANDERSPOEL, A. Sijbers, H. Keegstra, and M. Renardus, GROMACS—a parallel computer for molecular-dynamics simulations, in *Proceedings of the 4th International Conference on Computational Physics (PC 92)* (World Scientific Publishing, Singapore, 1993), pp. 252–256.
- [37] G. Bussi, D. Donadio, and M. Parrinello, Canonical sampling through velocity rescaling, *J. Chem. Phys.* **126**, 014101 (2007).
- [38] M. Parrinello and A. Rahman, Polymorphic transitions in single crystals: A new molecular dynamics method, *J. Appl. Phys.* **52**, 7182 (1981).
- [39] R. W. Hockney, S. Goel, and J. Eastwood, Quiet high-resolution computer models of a plasma, *J. Comput. Phys.* **14**, 148 (1974).
- [40] T. Darden, D. York, and L. Pedersen, Particle mesh Ewald: An $n \log(n)$ method for Ewald sums in large systems, *J. Chem. Phys.* **98**, 10089 (1993).
- [41] U. Essmann, L. Perera, M. L. Berkowitz, T. Darden, H. Lee, and L. G. Pedersen, A smooth particle mesh Ewald method, *J. Chem. Phys.* **103**, 8577 (1995).
- [42] B. Hess, H. Bekker, H. J. Berendsen, and J. G. Fraaije, LINCSES: A linear constraint solver for molecular simulations, *J. Comput. Chem.* **18**, 1463 (1997).
- [43] J. R. Espinosa, C. Vega, C. Valeriani, and E. Sanz, Seeding approach to crystal nucleation, *J. Chem. Phys.* **144**, 034501 (2016).
- [44] I. Sanchez-Burgos, A. R. Tejedor, C. Vega, M. M. Conde, E. Sanz, J. Ramirez, and J. R. Espinosa, Homogeneous ice nucleation rates for mW and TIP4P/ICE models through lattice mold calculations, *J. Chem. Phys.* **157**, 094503 (2022).
- [45] I. Sanchez-Burgos, A. Garaizar, C. Vega, E. Sanz, and J. R. Espinosa, Parasitic crystallization of colloidal electrolytes: Growing a metastable crystal from the nucleus of a stable phase, *Soft Matter* **17**, 489 (2021).
- [46] I. S. Joung and T. E. Cheatham III, Determination of alkali and halide monovalent ion parameters for use in explicitly solvated biomolecular simulations, *J. Phys. Chem. B* **112**, 9020 (2008).
- [47] G. A. Orozco, O. A. Moulton, H. Jiang, I. G. Economou, and A. Z. Panagiotopoulos, Molecular simulation of thermodynamic and transport properties for the H₂O + NaCl system, *J. Chem. Phys.* **141**, 234507 (2014).
- [48] A. Benavides, J. Aragonés, and C. Vega, Consensus on the solubility of NaCl in water from computer simulations using the chemical potential route, *J. Chem. Phys.* **144**, 124504 (2016).
- [49] J. Espinosa, J. Young, H. Jiang, D. Gupta, C. Vega, E. Sanz, P. G. Debenedetti, and A. Z. Panagiotopoulos, On the calculation of solubilities via direct coexistence simulations: Investigation of NaCl aqueous solutions and Lennard-Jones binary mixtures, *J. Chem. Phys.* **145**, 154111 (2016).
- [50] Z. Mester and A. Z. Panagiotopoulos, Temperature-dependent solubilities and mean ionic activity coefficients of alkali halides in water from molecular dynamics simulations, *J. Chem. Phys.* **143**, 044505 (2015).
- [51] F. Moučka, I. Nezbeda, and W. R. Smith, Molecular force fields for aqueous electrolytes: SPC/E-compatible charged LJ sphere models and their limitations, *J. Chem. Phys.* **138**, 154102 (2013).
- [52] I. Nezbeda, F. Moučka, and W. R. Smith, Recent progress in molecular simulation of aqueous electrolytes: Force fields, chemical potentials and solubility, *Mol. Phys.* **114**, 1665 (2016).
- [53] J. Kolafa, Solubility of NaCl in water and its melting point by molecular dynamics in the slab geometry and a new BK3-compatible force field, *J. Chem. Phys.* **145**, 204509 (2016).
- [54] C. Perego, M. Salvalaglio, and M. Parrinello, Molecular dynamics simulations of solutions at constant chemical potential, *J. Chem. Phys.* **142**, 144113 (2015).
- [55] T. Karmakar, P. M. Piaggi, C. Perego, and M. Parrinello, A cannibalistic approach to grand canonical crystal growth, *J. Chem. Theory Comput.* **14**, 2678 (2018).

- [56] A. Stukowski, Visualization and analysis of atomistic simulation data with OVITO—the open visualization tool, *Model. Simul. Mater. Sci. Eng.* **18**, 015012 (2009).
- [57] W. Lechner and C. Dellago, Accurate determination of crystal structures based on averaged local bond order parameters, *J. Chem. Phys.* **129**, 114707 (2008).
- [58] N. E. Zimmermann, B. Vorselaars, D. Quigley, and B. Peters, Nucleation of NaCl from aqueous solution: Critical sizes, ion-attachment kinetics, and rates, *J. Am. Chem. Soc.* **137**, 13352 (2015).
- [59] G. Wulff, XXV. Zur frage der geschwindigkeit des wachstums und der auflösung der krystallflächen, *Z. Kristallographie-Crystalline Mater.* **34**, 449 (1901).
- [60] J. M. Rahm and P. Erhart, Wulffpack: A PYTHON package for Wulff constructions, *J. Open Source Software* **5**, 1944 (2020).
- [61] D. Aquilano, L. Pastero, M. Bruno, and M. Rubbo, $\{100\}$ and $\{111\}$ forms of the NaCl crystals coexisting in growth from pure aqueous solution, *J. Cryst. Growth* **311**, 399 (2009).
- [62] Y. Mu, A. Houk, and X. Song, Anisotropic interfacial free energies of the hard-sphere crystal-melt interfaces, *J. Phys. Chem. B* **109**, 6500 (2005).
- [63] R. Benjamin and J. Horbach, Crystal-liquid interfacial free energy of hard spheres via a thermodynamic integration scheme, *Phys. Rev. E* **91**, 032410 (2015).
- [64] F. Schmitz and P. Virnau, The ensemble switch method for computing interfacial tensions, *J. Chem. Phys.* **142**, 144108 (2015).
- [65] B. B. Laird, R. L. Davidchack, Y. Yang, and M. Asta, Determination of the solid-liquid interfacial free energy along a coexistence line by Gibbs-Cahn integration, *J. Chem. Phys.* **131**, 114110 (2009).
- [66] P. Montero de Hijes, J. R. Espinosa, V. Bianco, E. Sanz, and C. Vega, Interfacial free energy and toman length of curved liquid-solid interfaces from equilibrium studies, *J. Phys. Chem. C* **124**, 8795 (2020).
- [67] M. Quilaqueo and J. M. Aguilera, Crystallization of NaCl by fast evaporation of water in droplets of NaCl solutions, *Food research international* **84**, 143 (2016).